Coincident Time-of-Flight Measurements of the Velocities of Fission Fragments from Charged-Particle-Induced Fission*

STANLEY L. WHETSTONE, JR.

Los Alamos Scientific Laboratory, University of California, Los Alamos, New Mexico

ABSTRACT

Measurements have been made of the velocities of the two coincident fission fragments emitted in the 25.7- and 29.7-MeV He^4-induced fission of U^{233} and Th^{230}, the 25.7- and 29.5-MeV He^4-induced fission of Th^{232}, and the 12.0- and 14.0-MeV H^2-induced fission of Th^{230}. Previously unpublished data for the 21.8-MeV He^4-induced fission of U^{233} and Th^{232} are also included. The resulting distributions of fragment masses and kinetic energies are consistent with the hypothesis of two competing modes of fission. Comparison of the primary mass yields determined in the present work with the yields determined by radiochemical methods indicates a dependence of neutron emission on fragment mass, which is

* Work performed under the auspices of the U. S. Atomic Energy Commission.

DISCLAIMER

consistent with the expectations of a two-mode neck model. In the course of correcting the time-of-flight mass distributions for the influence of the prefission neutron emission and the detection solid angle, approximate dependences of the yield of symmetric mass divisions on the excitation energy of the fissioning nuclei were estimated.

INTRODUCTION

When the measurements reported here were begun, there was experimental evidence[1,2] that the average amount of kinetic energy given to fission fragments was not always a maximum for the most symmetric mass divisions as is expected from the simplest theory. Apparently, there was a sudden and large decrease in the kinetic energy release for somewhat more symmetric mass divisions than those observed to be most probable. Since data were not available, however, for cases where the relative yield of symmetric mass divisions was appreciable, the experimental results were uncertain, chiefly because of the difficulty in making reliable corrections under these conditions for the dispersion of the measurements. Preliminary time-of-flight measurements[3] of charged-particle-induced fission, which give relatively large yields of symmetric mass divisions, showed that the kinetic energy release is indeed decreased by as much as 10 MeV over a large interval of fragment mass ratios near unity for fission at moderate excitation energy.

Recently, double-energy measurements were made with semiconductor detectors[4] of the fission of nuclides of lower fissionability where equally probable symmetric and asymmetric mass division and even predominantly symmetric mass divisions are observed. These measurements permitted a fairly precise analysis[4] in terms of two distinct components--one characterized by unequal mass divisions and higher kinetic energy releases, and the other, competing more favorably at higher excitation energies, by nearly

equal mass divisions and lower kinetic energy releases. The present measurements investigate a number of reactions for which significant numbers of symmetric mass divisions are observed, using two initial excitation energies, and provide a further test of the two-mode hypothesis in the region of the more fissionable nuclides.

It now appears that time-of-flight measurements, as used in this study, are valuable chiefly because of their ability to measure distributions of fragment masses (and energies) equivalent to the distributions before the emission of prompt neutrons. It has been realized for some time that a comparison of initial mass distributions and radiochemical mass distributions provides information concerning the number of neutrons emitted. Terrell[5] has recently devised a convenient way to make this comparison, so that the dependence of the neutron emission from individual fragments on the fragment mass can be determined. (Terrell has also shown[5] how time-of-flight double-velocity data can be compared with double-energy data to obtain similar information concerning prompt neutron emission. Such a comparison is treated in a companion paper.[6])

To make the time-of-flight data compatible with the radiochemical data, in view of the different detection solid angles used, it was necessary to consider the effects of prefission neutron emission and the dependence of the mass and angular distributions of the fragments on the excitation energy of the fissioning nucleus. Approximate dependences of the yield of symmetric mass divisions on the excitation energy of the fissioning nuclei were determined.

EXPERIMENTAL

Apparatus

A schematic diagram of the detection system, including the pertinent dimensions, is given in Fig. 1. The detectors and electronic systems were the same as those used for the Cf^{252} spontaneous fission measurements.[7] The target foil was oriented at 45° to both the cyclotron beam and fragment flight paths, and because of space limitations the fragment flight paths were shorter than those used in the spontaneous fission measurements. Electron-lens-type fragment detectors were placed slightly forward of the target to detect fragment pairs emitted at approximately 90° to the beam in the c.m. system (assuming absorption of the incident particles to form compound nuclei). The terminal detector for fragments passing through the source backing and initial-lens foil had an 19.7-cm-diameter aperture, and the other terminal detector, 10.2 cm. The numbers of heavy and light fragments detected in each of the detectors were more nearly equal than was found in the previous Cf^{252} work,[7] perhaps because of the larger solid angles. The time converters were started by pulses from the remote fragment detectors. The trigger rates of the time-converter discriminators were monitored continuously during the runs.

Targets

Targets of U^{233}, Th^{232}, and Th^{230} were used. The U^{233} target consisted of ~20 $\mu g/cm^2$ of the fluoride (~99% U^{233}) vacuum-evaporated on 2.5×10^{-6} in. Ni foil; the Th^{232} consisted of ~40 $\mu g/cm^2$ of the fluoride (~100% Th^{232}) vacuum-evaporated on 4.0×10^{-6} in. Ni foil; and the Th^{230} consisted of ~ 20 $\mu g/cm^2$ of the oxide (90.2% Th^{230},

9.8% Th^{232}) electrosprayed on 5.0 x 10^{-6} in. Ni foil. (Nickel foil thicknesses quoted are nominal values.)

Incident Beams

The cyclotron beam was collimated to produce a spot about 3 mm in diameter at the targets. The beam energies were measured and monitored at frequent intervals by scattering the beam into a semiconductor detector through a thickness of Al absorber sufficient to produce the same pulse height as the 5.14-MeV alphas from a Pu^{239} calibration source. Absolute determination of energy to better than ±0.05 MeV is claimed for the system,[8] although the energy was allowed to vary by ±0.20 MeV during the present runs. Alpha and deuteron beam intensities through the targets were held to about 12 nanoamperes for all of the reactions to prevent excessive counting rates in the initial detector.

Calibration and Velocity Loss Corrections

Interspersed with the particle-induced fission measurements were a number of measurements of the spontaneous fission of Cf^{252} in the same apparatus (with the terminal detectors put in line with the source). It was possible to find a zero-time difference for each of the two recording channels which, with an estimate of the velocity loss correction in one of the fragment directions, gave cumulated velocity distributions that were the same as the distribution determined in the earlier precision Cf^{252} measurements,[7] except for an apparently slightly larger dispersion. These two zero-time differences were then used to determine the velocity distributions for all of the particle-

induced fission reactions. Velocity corrections for individual target foils were determined by comparison of the cumulated velocity distributions in the two fragment directions, the same velocity correction being used for a given target. It is possible that a small systematic error is introduced in the calibration through small differences in the pulse heights from fragments of a given velocity from Cf^{252} and from the lower-mass fissioning nuclei studied in this work.

Resolution

Direct measurements of the zero-times, by moving a terminal detector close to the target, were not made for particle-induced fissions, and therefore no direct measurements of the actual time resolutions are available. Such measurements were made,[7] however, with a Cf^{252} source before the cyclotron runs, which yielded a standard deviation of the time distribution for fragments of a given velocity $\sigma(T) = 0.95 \pm 0.15$ nsec (2.2 ± 0.3 nsec FWHM).[9] Measurements were made with a Cf^{252} source in He^4 beams of different intensities and a terminal detector brought up to 26.0 cm from the initial detector foil. These measurements, with the electronic system adjusted for tolerable counting rates in the detectors, indicated somewhat larger time dispersions than those found previously, but almost no dependence on beam intensity in the range used in the present experiments. On the basis of these measurements, the time resolution for the particle-induced fissions is estimated to have been $\sigma(T) = 1.3 \pm 0.3$ nsec (3.0 ± 0.6 nsec FWHM). Therefore, the percentage resolutions $\sigma(V)/V$ of the heavy and light fragment velocity measurements are $0.85 \pm 0.13\%$ and $1.2 \pm 0.2\%$, respectively, ($2.0 \pm 0.3\%$ and $2.8 \pm 0.4\%$ FWHM); and

the mass resolution, including the effects due to the emission of 4.5 ± 1.0 prompt neutrons per fission, is $\sigma(A_F)$ = 1.2 ± 0.2 amu (2.8 ± 0.4 amu FWHM). Instrumental effects contributed about the same amount to the total dispersion of the measurements as did the effects of neutron emission.

The method used to remove dispersive effects from the distributions is described briefly in Appendix A.

RESULTS

Table I lists the reactions studied and the means and standard deviations of the observed distributions. The data obtained in the previous work[3] at 21.8-MeV incident alpha energy are included, because these measurements were not repeated in the present work.[10]

When the data were analyzed into V_1 x V_2 and E_1 x E_2 matrixes, it was clear that a relatively large background of obviously spurious events occurred even in regions well removed from the bulk of the events. The presence of these events had an understandably large effect on the observed standard deviations of the velocity and energy distributions; and, in addition, the dependence of $\langle E_K(R_A) \rangle$ was found to suffer unreasonable fluctuations, particularly in the regions of lower yield at the larger values of mass ratio. Since these outlying events were much more uniformly distributed with respect to mass, the mass distributions were much less strongly affected. After some trials, it was decided that it would be advisable to require all of the data to fulfill the following requirements: $0.72 \leq V \leq 1.68$; $2.08 \leq V_1 + V_2 \leq 2.68$; and $-1.60 \leq V_1 - V_2 \leq 1.60$, in units of cm/nsec.

Distributions in fragment velocity, mass, and kinetic energies are shown in Figs. 2 to 4. Mass-ratio distributions and mass-ratio

dependences of the means and standard deviations of the conditional total kinetic energy distributions are shown in Figs. 5 to 8.

DISCUSSION

The mass distributions in Fig. 3 all display the preference for asymmetric mass divisions expected for these highly fissionable nuclides. The average total fragment kinetic energies in Figs. 7 and 8 show the now accepted decrease toward the symmetric mass ratio. The alpha-particle-induced reactions show the usual increase in yield of the more symmetric mass divisions with an increase of bombarding energy.[11] With varying degrees of certainty, the mass-ratio dependence of the average total kinetic energy is seen to change with bombarding energy in the region of mass ratios intermediate between the symmetric and most probable mass divisions; this is in general agreement with the proposal by Britt et al.[4] of a second distinct mode of fission (characterized not only by a preference for symmetric mass division but also by a lower total kinetic energy release) which contributes increased fission yield as the excitation energy is increased. For each reaction a peak of some kind is observed in the widths $\sigma(E_K)$ of the conditional total kinetic energy distributions, which has been interpreted[4] as evidence of overlapping energy distributions from the two modes in the intermediate mass-ratio region.

The fragment velocity distributions of Fig. 2 show clearly a double-peaked light fragment group. The smaller peak occurs at lower velocities and undoubtedly corresponds to events of nearly symmetric mass division and lower kinetic energy, as ascribed to the symmetric mass division component. The heavy fragment symmetric mass division component peak must be largely hidden in the high velocity wing of the

heavy fragment velocity peak. The dependence of the velocity distributions on excitation energy is again in accord with the two-mode picture.

The U^{233} distributions, which show relatively smaller decreases in $\langle E_K(R_A)\rangle$ toward $R_A = 1$, smaller changes in $\langle E_K(R_A)\rangle$ with bombarding energy, and a more dispersed peak in $\sigma(E_K)$, may indicate that asymmetric mass division is contributing significantly to the symmetric mass divisions. The smaller most probable mass ratio for U^{233}, which is the heaviest fissioning nuclide studied here, makes this plausible. It is also possible that the U^{233} reaction gives somewhat different results simply because a larger fraction of the fissions occur prior to the emission of neutrons and, therefore, at higher average excitation energies.

The results of the deuteron-induced fission of Th^{230} appear to show less sensitivity to the bombarding energy, and, in fact, show a slight reversal of the expected dependence of mass yield and average kinetic energy release on excitation energy. The yield of symmetric mass divisions is actually slightly decreased, and the kinetic energy release slightly increased, at the higher excitation energy. This is probably because the lower of the two incident energies is at or just below the threshold for the relatively strongly contributing third-chance fission, while the higher incident energy is no more than 2.0 MeV above it. (See Table II.)

Yield of Symmetric Mass Divisions as a Function of Excitation Energy

The results obtained in this experiment are complicated by the fact that in none of the reactions studied do the products come from

the fission of a single nuclear species, but in each case it is, on the average, possible for fission to occur after the evaporation of a neutron. In particular, each observed mass distribution results from a superposition of two or more distributions corresponding to the members of the chain of fissioning nuclides that can be produced by successive prefission neutron emission. One can expect the superposed mass distributions to be different, because the average excitation energy of each successive member of the chain is lowered by the energy lost to the neutron, and because it is known from data obtained at low initial excitation energies that the shape of the mass distributions (in particular the proportion of symmetric to asymmetric mass division) is strongly dependent on the excitation energy. It is also known that the angular distribution of the emitted fragments with respect to the incident beam of particles is dependent on the excitation energy. Therefore, observation in a limited solid angle will, in general, not include the same proportions of first-, second-, and third-chance fission events.

In the present section, estimates are made of the dependence of the yield from symmetric mass division on the excitation energy of the fissioning nucleus, assuming that this yield is relatively insensitive to small changes in neutron number. A complete mass distribution for fission of a given nuclide at a given excitation energy can be generated by making the further assumption that the distributions can be analyzed into two component distributions, one of them a normal distribution of a given width with mean value at symmetric mass, the other with no yield at the symmetric mass.[12] This information is then used in the next section to convert the mass distributions observed in this

experiment (in a small solid angle at 90° to the beam) to those expected to be found in the total solid angle, so that a comparison can be made with the various mass distributions determined by radiochemical means.

The observed total yields of symmetric mass division for each initial excitation energy E_{x1} are given in Fig. 9(b). These yields (at an observed angle θ_o to the beam) can be expressed by $y(M_s,\theta_o) = \Sigma\, k_i y_i(M_s,\theta_o)$; $\Sigma\, k_i = 1$, where k_i, $i = 1, 2, \ldots$ are the fractions of the fissions occurring after the emission of $(i - 1)$ neutrons, $y_i(M_s,\theta_o)$ are the corresponding partial symmetric mass yields corrected for dispersive effects, and the summation is over the chain of nuclides contributing to fission. The evaluation of the fission fractions k_i is described in Appendix B. Values of the excitation energies E_x and the fraction of fissions occurring at each stage are included in Table II.

The excitation-energy dependence of the symmetric yield derived from the measurements is shown in Fig. 9(b). A simple iterative procedure was used to determine the $y_i(M_s,\theta_o)$. Upper limits to the partial yields at excitation energies corresponding to the initial excitation energies from each measurement can be obtained if one assumes that all of the symmetric yield is from first-chance fission. Minimum limits to the partial yields are then obtained by assuming that the true dependence of the partial yields is given by a curve drawn through the upper limits just calculated. The partial yields at excitation energies below the second-chance fission threshold at about 12 MeV are obtained from the radiochemical data of Ford and Gilmore,[13] which are also given in reference 14, converted to absolute percent yields in Fig. 6. The lower fission threshold for U^{233} + He^4 suggests the use of a similar

curve displaced to smaller excitation energies. This procedure determines quite uniquely the dependence of each of the partial yields. When the symmetric yields observed at 90° to the beam are converted in an approximate manner (described in the next section) to the yields expected in the total solid angle $Y(M_s)$, as shown by the solid curves in Fig. 9(b), the dependences still are not identical for the various reactions, indicating a possible dependence on the nucleonic constitution of the fissioning nuclide. When the observed radiochemical yield ratios of Cd^{115}/Mo^{99} shown in Fig. 9(a) are treated in the same way, however, the two sets of data for the initial compound nucleus U^{236*} do not agree either, although the shapes of the curves are quite similar.

Each mass distribution can be assumed to be the sum of two distributions. The component that includes the more symmetric mass divisions is a normal distribution with mean at the symmetric mass M_s and maximum value equal to the symmetric mass yield $y(M_s)$ since the other component is assumed to contribute negligibly to the symmetric mass yield. For a standard deviation of 9.3 amu, the same width[15] as that observed for the large central component of the mass distribution from the fission of Ra^{226} by 11.7-MeV deuterons,[4] the normalization of the total mass distribution to 200% yield corresponds to a total percentage central component yield approximately equal to $23.4\ Y(M_s)$. The maximum possible yield of the symmetric mass would be about 8% (corresponding to no contribution from the component that includes predominantly asymmetric mass division). The indicated leveling-off of all of the partial symmetric yields (Fig. 9) at about 4%, corresponding to approximately

equal amounts of the two components, is strongly suggestive of the behavior predicted for separate fission barriers for the two modes. The barrier for the central mode lies at a somewhat higher energy than the barrier for the other mode.[16, 11]

Prompt Neutron Emission as a Function of Fragment Mass

Terrell[5] has shown that the comparison by means of cumulated distributions of the primary mass yields, determined from time-of-flight measurements, and the secondary mass yields, determined by radiochemical methods, should permit an accurate determination of the average number of prompt neutrons emitted from fragments as a function of the fragment mass. This procedure depends, of course, on the availability of sufficiently accurate data of the two kinds--which is probably just barely the case at present. Nevertheless, in view of the potentially important information concerning the basic fission process that is contained in the neutron data, and the difficulty in obtaining this information by direct measurement, it is felt that the available data, in spite of its uncertainty, should be investigated. Such an investigation, in which the neutron emission behavior is extracted from a comparison of the time-of-flight and solid state detector mass distributions, is being made.[6] This latter method is independent of the uncertainties introduced by the sparse and relatively uncertain radiochemical measurements, and has the advantage of possible cancellations of some of the systematic errors, but it involves a more difficult and approximate analysis.

Before the time-of-flight mass distributions are compared to the radiochemical mass yields, they must be corrected for resolution, the

effect of the different detection solid angle, and the decrease in the average mass of the fissioning nucleus.

The resolution correction was performed by the method described in Appendix A which both smooths, by a least squares procedure, and unfolds the experimental dispersion.

The correction for the solid angle and mass shift effects is described in the following. Using the analysis of the mass distributions described above, the effect of the detection solid angle on the observed mass distributions can be simply, though crudely, estimated from the following expressions for the total yield of the symmetric mass in the total solid angle $Y(M_s)$ and the corresponding yield at an angle θ_o to the beam $y(M_s,\theta_o)$:

$$Y(M_s) = \Sigma k_i Y_i(M_s)$$

$$y(M_s,\theta_o) = \Sigma k_i Y_i(M_s) F_i(\theta_o)/\Sigma k_i F_i(\theta_o),$$

where the summations are over the number of nuclides, each at a different excitation energy, contributing to the total fission yields; k_i, normalized to unity, is the fraction of the fissions contributed by each member of the chain of nuclides; $F_i(\theta_o)$ is the ratio of the partial yields at angle θ_o to the partial yields averaged over the total solid angle. The assumption has been made that the partial mass and angular distributions are independent. Evaluation of $F_i(\theta_o)$ is discussed in Appendix C; the resultant values are included in Table II. As a first approximation, the values found above for the partial symmetric mass yields [Fig. 9(b)] can be substituted for the $Y_i(M_s)$ in the above equations to obtain the ratios of the yields $Y(M_s)/y(M_s,90^o)$. The ratios for

29.7-, 25.7-, and 21.8-MeV alphas on U^{233} are calculated to be 0.98, 0.96, and 0.97; for 29.5-, 25.7-, and 21.8-MeV alphas on Th^{232} they are 0.95, 0.91, and 0.95; for 29.7- and 25.7-MeV alphas on Th^{230} they are 0.96 and 0.92; and for 14.0- and 12.0-MeV deuterons on Th^{230} they are 0.95 and 0.99. The small size of the corrections helps to justify the many approximations used in their derivation. The time-of-flight mass distributions are analyzed into symmetric and asymmetric component distributions, each symmetric component distribution multiplied by the appropriate factor $Y(M_s)/y(M_s,90^o)$; each asymmetric component, by a factor to preserve the normalization.

The correction for the decrease in the average mass of the fissioning nucleus can be made by noting that the measured mass ratio obtained from the ratio of the measured velocities is, on the average, independent of the mass of the fissioning nucleus. Therefore, the mass shift is given by $\Delta M_L/M_H = \Delta M_H/M_H = \Delta M/M$, where the magnitude of ΔM is obtained directly from the fission fractions k_i. Since the symmetric component receives by far its greatest contribution from first-chance fission, only the asymmetric component distribution is shifted.

The results of the comparison of the corrected time-of-flight data and radiochemical data for the reaction $U^{233} + He^4$ at incident energies near 25.5 and 29.0 MeV are shown in Fig. 10. The mass distribution published by Colby et al.[17] implies a wildly varying neutron emission, reaching impossible negative values in the region of mass number $A_F = 130$. The recent data of R. D. Fink,[18] at 25.3 MeV, although showing qualitatively the same type of oscillatory dependence

of $\langle \nu_F(A_F) \rangle$, would imply that the variations are much smaller. The effects of uncertain knowledge of the radiochemical yields on the determination of the mass dependence of neutron emission is graphically illustrated. Figure 11 shows the results of the comparison of the fission of Th^{232} by 25.7-MeV alphas and the radiochemical data from the reaction U^{235} + 14-MeV neutrons,[19] which produces the same initial compound nucleus U^{236*} at almost the same excitation energy. The dependence $\langle \nu_F(A_F) \rangle$ is strikingly similar to that found, using the data of Fink,[18] for fission following from the initial compound nucleus Pu^{237*} at a similar initial excitation energy. It is possible, however, that in both cases the radiochemical yields are systematically in error in the same way. The peaks in neutron emission near mass $A_F = 105$ could be generated by systematically low measurements of radiochemical yields in this mass region. The matching dips in neutron emission near mass $A_F = 130$ follow, to a large degree, from the assumption of reflection symmetry about mass number $A_F = (A_T - \langle \nu_T \rangle)/2$, which is assumed to be a first-order means for interpolating the missing radiochemical yields.

The dependence of neutron emission indicated by the solid curves of Figs. 10 and 11 is consistent with the expectation of the two-mode neck model. The predominant mode of asymmetric mass division is characterized by an asymmetric dumbbell which, on breaking in two, divides the neck and the associated deformation energy between the two fragments, giving rise to the usual "sawtooth" behavior observed at low excitation energies. The mode of nearly symmetric mass division, characterized by a symmetric dumbbell (which can no longer distinguish between its ends), gives rise to a monotonic increase in neutron emission with fragment mass. The superposition of the two would be expected to smooth the sawtooth dependence, and perhaps even yield the gradually rising

plateau observed near symmetric mass divisions.

The comparison between these time-of-flight measurements and double-energy measurements made with semiconductor detectors, which is reported in an accompanying paper,[6] indicates a similar neutron emission, but without the pronounced peak and dip. It can indeed be shown that this smoothed-out dependence is consistent with radiochemical measurements assigned fairly large uncertainties, so that the pronounced structure reported here is not very certain. The structure observed here is more like that which would be expected from current statistical treatments of the fission process, which closely link the mass yield with the fragment excitation and kinetic energy release.[20]

ACKNOWLEDGMENTS

I am grateful to R. B. Leachman for suggesting that these measurements be made, for making available the cyclotron, and for his active participation in the early experimental measurements. Judith Gursky prepared the electrosprayed Th^{230} source, J. G. Povelites prepared the vacuum-evaporated targets, and K. R. Crandall and W. S. Hall assisted with the computer codes. I am indebted to H. C. Britt and J. Terrell for many valuable discussions concerning interpretation of the data.

APPENDIX A

Resolution Correction

Dispersive effects can be removed from an observed distribution by a point-by-point procedure if the resolved curve can be adequately represented by a polynomial of sufficiently low degree over an interval larger than that affected by the dispersion function. If the dispersion function $D(x - x')$ is assumed to be Gaussian with a variance σ^2, and the resolved curve is considered to be represented adequately in intervals of width $\sim 6\sigma$ by a polynomial of degree n, where $2n + 1$ is sufficiently smaller than the number of points in the distribution, then the solution of the folding integral

$$Y(x) = \int_{-\infty}^{\infty} y(x')D(x - x')dx' / \int_{-\infty}^{\infty} D(x - x')dx'$$

provides relations between the coefficients a, b, ... of the resolved curve and coefficients A, B, ... of a polynomial representing the observed data. For $n = 3$,

$$a = A - C\sigma^2,\ b = B - 3D\sigma^2,\ c = C,\ d = D.$$

The values of A, B, ... are determined from a least squares fit of a polynomial of degree n to a sufficiently large number of data points centered on the point to be corrected. The corrected value of each point is taken to be the value of the respective resolved curve at that point. Extrapolations must be made at both ends of the distribution. This procedure is well adapted to computer computation, and the least squares fitting helps smooth out statistical fluctuations.

The present mass distributions were corrected using n = 3 and nine points for each fit.

The above procedure has been extended to permit the more difficult correction of regression curves, such as $\langle \nu_F(R_A) \rangle$ for dispersion in the parameter R_A: in other words, to solve the equation $\nu_o(x) = \int_{-\infty}^{\infty} \nu_T(x')N(x')D(x - x')$: $\int_{-\infty}^{\infty} N(x')D(x - x')dx'$ for $\nu_T(x')$.

APPENDIX B

Calculation of the k_i

The fission fractions k_i were obtained for each reaction by considering only the competition between fission and neutron emission at each step in the de-excitation of the initial compound nucleus. The appropriate values of Γ_f/Γ_n, the ratio of the fission width to neutron width, taken from a smooth curve drawn through the plot of Γ_f/Γ_n vs Z^2/A given by Halpern and Coffin,[21] were used to determine the "fractional fissionabilities"[22] $f_i = (\Gamma_f/\Gamma_n)_i/[1 + (\Gamma_f/\Gamma_n)_i]$. Dependence of Γ_f/Γ_n on the excitation energy, which is expected to be small for the relatively highly fissionable nuclides considered here, was ignored, as were possible small angular momentum effects. The average excitation energy E_x of each nuclide in the chain was then determined successively, beginning with the initial compound nucleus, for which $E_x = 0.98\ E_\alpha - S_\alpha$, where E_α is the kinetic energy of the incident alpha particle, and S_α is the separation energy of an alpha particle in the compound nucleus. The average excitation energy after the emission of a neutron is given by $E_s(i) = E_x(i - 1) - S_n(i - 1) - E_n(i - 1)$, where $S_n(i - 1)$ is the neutron separation energy in the preceding nucleus, and $E_n(i - 1)$ is

the average emission energy of the neutrons. For an evaporation spectrum, $\bar{E}_n(i-1) = 2T(i) = 2(\{1 + a[E_x(i-1) - S_n(i-1)]\}^{1/2} - 1)/a$.[23] When the excitation energy decreases to below the fission threshold (~5 MeV), the chain of fission nuclides is terminated. Because of the poor definition of the fission threshold and the spread in excitation energies induced by the spectrum of neutron emission energies, a probably more accurate estimate of the length of the chain is obtained by observing the effect on the angular distributions of the fragment yields, where they have been measured. The data of reference 24 indicate that third-chance fission is fully developed for Th^{232} + 25.7-MeV He^4. The He^4-induced fission of U^{233} gives too small a fraction of third-chance fission for the effects of the thresholds to be noticeable in the angular distributions, and their importance in the present analysis is similarly small. Better consistency is obtained if it is assumed that this threshold is reached in the U^{233} and Th^{230} + He^4 reactions, but not in the Th^{230} + H^2 reaction. The fact that the threshold is exceeded in these cases by some unknown fraction of events adds some uncertainty to the analysis. Finally, knowing the length m of the fissioning chain, the fission fractions k_i are calculated for each reaction from the fractional fissionabilities, so that $k_i = 1$, summed for i = 1, m. (See Table II.)

APPENDIX C

Calculation of the $F_i(\theta_o)$

The factors $F_i(\theta_o) = 2W_i(p,\theta_o) / \int_o^\pi W_i(p,\theta)\sin\theta d\theta$ are calculated from the angular distributions $W(p,\theta)$ given by Halpern and Strutinski.[22] The

parameter $p = (I_m/2K_o)^2$ depends on the kinetic energy E_α of the incident alpha particle and the excitation energy $E_x(i)$ of the fissioning nucleus. The maximum value I_m of the angular momentum I deposited in the compound nucleus is calculated from an approximate relation also given by Halpern and Strutinski: $I_m^2 = 20.6(E_\alpha - 17.6)$ and $I_m^2 = 11.3(E_d - 10)$, with E_α and E_d in MeV. It is assumed that the angular momentum is not changed appreciably by neutron emission. K_o^2 is the average of the square of the projection of I on the symmetry or separation axis of the fissioning nucleus. The dependence of K_o^2 on the excitation energy has been determined from angular distribution measurements by Vandenbosch, Warhanek, and Huizenga.[24] The values of the quantities K_o^2 and the resulting factors $F_i(90^\circ)$ are given in Table II.

TABLE I. Mean values and standard deviations of the observed distributions.[a]

Target	U^{233}	U^{233}	U^{233}[b]	Th^{232}	Th^{232}	Th^{232}[b]	Th^{230}	Th^{230}	Th^{230}	Th^{230}
Projectile	He^4	He^4	He^4	He^4	He^4	He^4	He^4	He^4	H^2	H^2
E_{inc}(MeV)	29.7	25.7	21.8	29.5	25.7	21.8	29.7	25.7	14.0	12.0
No. of events	8,843	22,111	11,398	3,746	3,233	9,959	13,805	16,353	19,765	22,381
$\langle V_L \rangle$(cm/nsec)	1.369	1.380	1.404	1.378	1.391	1.410	1.369	1.383	1.408	1.404
$\langle V_H \rangle$(cm/nsec)	1.041	1.036	1.027	0.996	0.993	0.984	1.005	1.003	0.993	0.990
$\sigma(V_L)$(cm/nsec)	0.115	0.111	0.110	0.112	0.104	0.106	0.117	0.112	0.117	0.117
$\sigma(V_H)$(cm/nsec)	0.095	0.093	0.092	0.087	0.083	0.086	0.090	0.087	0.086	0.087
$\langle M_L \rangle$(amu)	102.4	101.7	100.2	99.1	98.3	97.0	99.2	98.4	96.1	96.1
$\langle M_H \rangle$(amu)	134.6	135.3	136.8	136.9	137.7	139.0	134.8	135.6	135.9	135.9
$\sigma(M_L)$(amu)	9.0	8.8	8.4	8.8	8.2	7.9	9.1	8.7	8.9	9.0
$\sigma(M_H)$(amu)	9.0	8.8	8.4	8.8	8.2	7.9	9.1	8.7	8.9	9.0
$\langle E_L \rangle$(MeV)	98.9	99.8	101.7	96.9	98.1	99.5	95.6	97.0	98.0	97.4
$\langle E_H \rangle$(MeV)	75.4	75.1	74.6	70.2	70.1	69.6	70.4	70.5	69.3	68.9
$\sigma(E_L)$(MeV)	9.9	9.6	9.8	9.2	8.6	9.9	9.6	9.3	9.1	9.1
$\sigma(E_H)$(MeV)	9.6	9.3	9.5	8.4	8.1	9.0	8.6	8.4	7.9	8.0
$\langle E_K \rangle$(MeV)	174.2	174.9	176.3	167.0	168.2	169.1	166.0	167.5	167.3	166.3
$\sigma(E_K)$(MeV)	14.6	14.2	15.1	12.8	12.4	15.5	13.2	12.9	11.5	11.6
$\langle R_A \rangle$	1.330	1.346	1.380	1.399	1.416	1.446	1.376	1.393	1.433	1.432
$\sigma(R_A)$	0.209	0.205	0.200	0.210	0.199	0.194	0.215	0.208	0.218	0.218

TABLE I. (Continued)

[a]The symbols L and H refer to the lighter or heavier of the pair of fragments as determined from the velocity ratio; V, M, and E refer to the fragment velocity, mass, and kinetic energy; E_K is the total kinetic energy; and R_A is the mass ratio. All velocities, masses, and kinetic energies are essentially those prior to the emission of the prompt neutrons. These values have been obtained assuming complete absorption of the projectile to form a compound nucleus, and no prefission neutrons. (See text for a discussion of the effects of the prefission neutron emission.) Absolute uncertainties (95% confidence limits) are estimated to be about ±1%, ±1%, and ±2% for the mean velocities, masses, and energies, respectively. Statistical uncertainties may be estimated from the standard deviations and numbers of events. Standard deviations listed are uncorrected for dispersive effects and are considered rather uncertain because of the presence of a significant background of spurious events. (See Results section.)

[b]These data are taken from the earlier work (see reference 3) and calibrated with respect to the present data. They contain a significantly larger instrumental dispersion. (See footnote 10.)

TABLE II. Multichance fission parameters.[a]

Target	Proj.	C. N.	E_{inc}	Chance fission ith	E_x	(k)[c]	k	E_F	$(K_o^2)^b$	F^b
U^{233}	He^4	Pu^{237}	21.8	1	15.8		0.76	4.6	67	0.958
		Pu^{236}	21.8	2	8.8		0.24	5.1	12	0.836
		Pu^{237}	25.7	1	19.6	(0.76)	0.72	4.6	90	0.940
		Pu^{236}	25.7	2	12.4	(0.24)	0.22	5.1	31	0.859
		Pu^{235}	25.7	3	(4.3)[c]	(0)	0.06	4.4	~0	0.637
		Pu^{237}	29.7	1	23.5		0.72	4.6	108	0.925
		Pu^{236}	29.7	2	16.1		0.22	5.1	66	0.887
		Pu^{235}	29.7	3	7.8		0.06	4.4	10	0.735
Th^{232}	He^4	U^{236}	21.8	1	16.7		0.57	5.6	67	0.958
		U^{235}	21.8	2	9.1		0.43	5.2	13	0.842
		U^{236}	25.7	1	20.6		0.43	5.6	90	0.940
		U^{235}	25.7	2	12.8		0.33	5.2	33	0.864
		U^{234}	25.7	3	6.5		0.24	5.5	2	0.680
		U^{236}	29.5	1	24.3		0.43	5.6	107	0.925
		U^{235}	29.5	2	16.3		0.33	5.2	67	0.888
		U^{234}	29.5	3	9.7		0.24	5.5	14	0.760
Th^{230}	He^4	U^{234}	25.7	1	20.4	(0.62)	0.51	5.5	89	0.939
		U^{233}	25.7	2	12.2	(0.38)	0.32	5.1	29	0.854
		U^{232}	25.7	3	(5.5)[c]	(0)	0.17	5.4	~0	0.637
		U^{234}	29.7	1	24.3		0.51	5.5	108	0.925
		U^{233}	29.7	2	15.9		0.32	5.1	64	0.884
		U^{232}	29.7	3	9.0		0.17	5.4	11	0.742
Th^{230}	H^2	Pa^{232}	12.0	1	20.0	(0.40)	0.53	5.7	86	0.992
		Pa^{231}	12.0	2	13.2	(0.34)	0.47	5.9	31	0.978
		Pa^{230}	12.0	3	(5.3)[c]	(0.26)	0	5.6	~0	0.637
		Pa^{232}	14.0	1	22.0		0.40	5.7	96	0.985
		Pa^{231}	14.0	2	15.1		0.34	5.9	48	0.970
		Pa^{230}	14.0	3	7.1		0.26	5.6	3.5	0.788

TABLE II. (Continued)

[a] E_{inc} = incident projectile kinetic energy (MeV), E_x = excitation energy of compound nucleus (MeV), k = fraction of first-, second-, and third-chance fission. E_F = fission threshold energy (MeV).

[b] See Appendix C.

[c] In these cases, it is uncertain whether or not the threshold for third-chance fission was exceeded.

FOOTNOTES

* Work performed under the auspices of the U. S. Atomic Energy Commission.

1. I. Halpern, Ann. Rev. Nuclear Sci. 9, 245 (1959).

2. E. K. Hyde, University of California Radiation Laboratory Report UCRL-9036, 1960, and UCRL-9036, Rev. 1962 (unpublished).

3. S. L. Whetstone and R. B. Leachman, Bull. Am. Phys. Soc. 6, 376 (1961).

4. H. C. Britt, H. E. Wegner, and J. C. Gursky, Phys. Rev. 129, 2239 (1963).

5. J. Terrell, Phys. Rev. 127, 880 (1962).

6. H. C. Britt and S. L. Whetstone, Jr. (to be published).

7. S. L. Whetstone, Jr., Phys. Rev. (to be published).

8. D. R. F. Cochran, Los Alamos Scientific Laboratory (private communication).

9. Uncertainties given in this section are roughly 95% confidence limits.

10. The previous results were reanalyzed and the calibration adjusted to make the mean velocities agree with the present values for the five measurements that were repeated. Because of a partial failure of one of the terminal detectors during the previous measurements, the instrumental dispersive effects were exceptionally large and the absolute calibration uncertain.

11. E. K. Hyde, University of California Radiation Laboratory Report UCRL-9065, 1960 (unpublished).

12. A similar analysis of high-energy proton-induced fission has been made by G. Rudstam and A. C. Pappas, Nuclear Phys. 22, 468 (1961).

13. G. P. Ford and J. S. Gilmore, Los Alamos Scientific Laboratory Report LA-1997, 1956 (unpublished).

14. H. G. Hicks, H. B. Levy, W. E. Nervik, P. C. Stevenson, J. B. Niday, and J. C. Armstrong, Jr., Phys. Rev. 128, 700 (1962).

15. No provision for a possible broadening of the mass distribution with increased excitation is considered necessary here. See reference 14.

16. W. M. Gibson, University of California Radiation Laboratory Report UCRL-3493, 1956 (unpublished).

17. L. J. Colby, Jr., M. L. Shoaf, and J. W. Cobble, Phys. Rev. 121, 1415 (1961).

18. R. D. Fink, PhD thesis, Massachusetts Institute of Technology, July 1962 (unpublished) and (private communication).

19. S. Katcoff, Nucleonics 18, No. 11, 201 (1960).

20. R. Vandenbosch, Nuclear Phys. (to be published). See also reference 5 and P. Fong, Bull. Am. Phys. Soc. II, 8, 385 (1963).

21. I. Halpern and C. T. Coffin, Proceedings of the Second International Conference on the Peaceful Uses of Atomic Energy, Geneva, 1958 (United Nations, Geneva, 1958), Vol. 15, p. 398.

22. I. Halpern and V. M. Strutinski, Proceedings of the Second International Conference on the Peaceful Uses of Atomic Energy, Geneva, 1958 (United Nations, Geneva, 1958), Vol. 15, p. 408.

23. J. Terrell, Phys. Rev. 113, 527 (1959).

24. R. Vandenbosch, H. Warhanek, and J. R. Huizenga, Phys. Rev. 124, 846 (1961).

FIGURE CAPTIONS

FIG. 1. Schematic diagram of the detection geometry. D_1 = 157.7 cm, D_1' = 7.6 cm, D_2 = 150.1 cm, A_1 = 19.7 cm diam, A_2 = 10.2 cm diam. INITIAL DETECTOR: 2-μin. Ni foil, 0.0005-in. NE102 fluor, RCA 6810A P.M. tube. TERMINAL DETECTOR(S): ~400 μg/cm^2 aluminized VYNS, 0.0005-mil NE102 fluor, RCA 7264 P.M. tube.

FIG. 2. Distributions of heavy and light fragment velocities as observed in a small solid angle corresponding to emission at approximately 90° to the incident beam in the c.m. system of the compound nucleus. No correction for dispersive effects (small) due to neutron emission or instrumental limitations.

FIG. 3. Observed distributions of fragment masses at 90° to the beam in the c.m. system. No correction for dispersive effects. Uncertainties shown are standard deviations based on the counting statistics. Fission is assumed to occur from the compound nucleus formed by complete absorption of the incident particle with no prefission neutron emission. The distributions therefore possess reflection symmetry through the dashed lines labeled "SYMMETRIC MASS."

FIG. 4. Distributions of heavy and light fragment kinetic energies at 90° to the beam in the c.m. system. Same assumption as Fig. 3. No corrections for dispersive effects. Uncertainties are standard deviations based on counting statistics.

FIG. 5. Observed widths (standard deviations) $\sigma(E_K)$ and means $\langle E_K \rangle$ of the total fragment kinetic energy distributions and the yields $Y(R_A)$ as functions of the mass division $R_A \equiv A_H/A_L$ for the alpha-particle-induced fission of U^{233} at incident energies 29.7, 25.7, and 21.8 MeV. The 21.8-MeV data are from the earlier work reported in reference 3. All observations are at 90° to the beam in the

c.m. system. No corrections for dispersive effects. Uncertainties are standard deviations based on counting statistics.

FIG. 6. Observed widths (standard deviations) $\sigma(E_K)$ and means $\langle E_K \rangle$ of the total fragment kinetic energy distributions and the yields $Y(R_A)$ as functions of the mass division $R_A \equiv A_H/A_L$ for the alpha particle-induced fission of Th^{232} at incident energies 29.5, 25.7, and 21.8 MeV. The 21.8-MeV data are from the earlier work reported in reference 3. All observations are at 90° to the beam in the c.m. system. No corrections for dispersive effects. Uncertainties are standard deviations based on counting statistics.

FIG. 7. Observed widths (standard deviations) $\sigma(E_K)$ and means $\langle E_K \rangle$ of the total fragment kinetic energy distributions and the yields $Y(R_A)$ as functions of the mass division $R_A \equiv A_H/A_L$ for the alpha particle-induced fission of Th^{230} at incident energies 29.7 and 25.7 MeV. All observations are at 90° to the beam in the c.m. system. No corrections for dispersive effects. Uncertainties are standard deviations based on counting statistics.

FIG. 8. Observed widths (standard deviations) $\sigma(E_K)$ and means $\langle E_K \rangle$ of the total fragment kinetic energy distributions and the yields $Y(R_A)$ as functions of the mass division $R_A \equiv A_H/A_L$ for the deuteron-induced fission of Th^{230} at incident energies 29.7 and 25.7 MeV. All observations are at 90° to the beam in the c.m. system. No corrections for dispersive effects. Uncertainties are standard deviations based on counting statistics.

FIG. 9(a). Observed total yields of the symmetric mass fragment for the reactions studied here and for some radiochemical experiments as functions of the excitation energy E_{x1} of the initially formed compound nucleus. The yields in the present work were observed in a small solid angle at approximately 90° to the incident beam in the c.m. system of the compound nucleus; the radiochemical yields were observed in the total solid angle. Yields are expressed as percentages of the total yield (200%). Corrections have been made in the present data for the small dispersive effects.

(b). Calculated partial yields of the symmetric mass fragment as functions of the average excitation energy E_x of the fissioning nuclide. Dashed curves represent yields at $\sim 90^{\circ}$ to the beam in the c.m. system; solid curves represent yields calculated for total solid angle, including corrections for the effects of anisotropic emission of the fragments.

FIG. 10(a). Distributions of the fragment masses $Y(A_F)$ before and after neutron emission from alpha-particle-induced fission of U^{233} as determined from the time-of-flight and radiochemical measurements. The distributions have been corrected for the dispersive effects of neutron emission and instrumental deficiencies and for the mass-shift produced by prefission neutron emission. In addition, the time-of-flight distributions measured at $\sim 90^{\circ}$ to the beam in the c.m. system have been converted to those expected in the total solid angle by correcting for the expected correlation between the mass yield and angle of emission. Dots and solid curve represent corrected primary mass distribution

in total solid angle. Squares, open circles, and heavier dashed curve represent measured secondary yields, yields obtained by reflection (assuming average total neutron emission $\langle \nu_T \rangle = 4.5$ neutrons), and the distribution obtained by interpolation and normalization to 200% total yield. Open triangles and lighter dashed curve are measured yields and yield curve as published by Colby et al., reference 17.

(b). The average number of neutrons emitted from fragments of a given mass $\langle \nu_F(A_F) \rangle$ as determined by comparison of mass distributions before and after neutron emission for alpha-particle-induced fission of U^{233}. Dots and solid curve represent comparison between corrected time-of-flight data at 25.7-MeV incident energy and data of R. D. Fink (reference 18) at 25.3 MeV. Heavier dashed curve is same time-of-flight data and data of Colby et al. (reference 17) at 25.3 MeV. Lighter dashed curve is corrected time-of-flight data at 29.7 MeV and data of Colby et al. at 29.0 MeV. Uncertainties are large and obviously very sensitive to uncertainties in the secondary mass distributions.

FIG. 11(a). Distributions of the fragment mass yields $Y(A_F)$ before and after neutron emission for fission reactions following the formation of the initial compound nucleus U^{236} at an excitation energy of approximately 20.6 MeV. See caption Fig. 10(a). Dots and solid curve represent corrected primary mass distribution in total solid angle for the fission of Th^{232} by 25.7-MeV alpha particles. Squares, open triangles, and dashed curve represent

measured secondary yields, yields obtained by reflection (assuming average total neutron emission $\langle \nu_T \rangle = 4$ neutrons), and the distribution obtained by interpolation and normalization (from the radiochemical data compiled by Katcoff, reference 20, for the fission of U^{235} by 14-MeV neutrons).

(b). The average number of neutrons emitted from fragments of a given mass $\langle \nu_F(A_F) \rangle$ as determined by the comparison of the mass distributions before and after neutron emission for fission following the formation of the initial compound nucleus U^{236*} at an excitation energy of approximately 20.6 MeV. Uncertainties are large.

Whetstone, Fig. 1

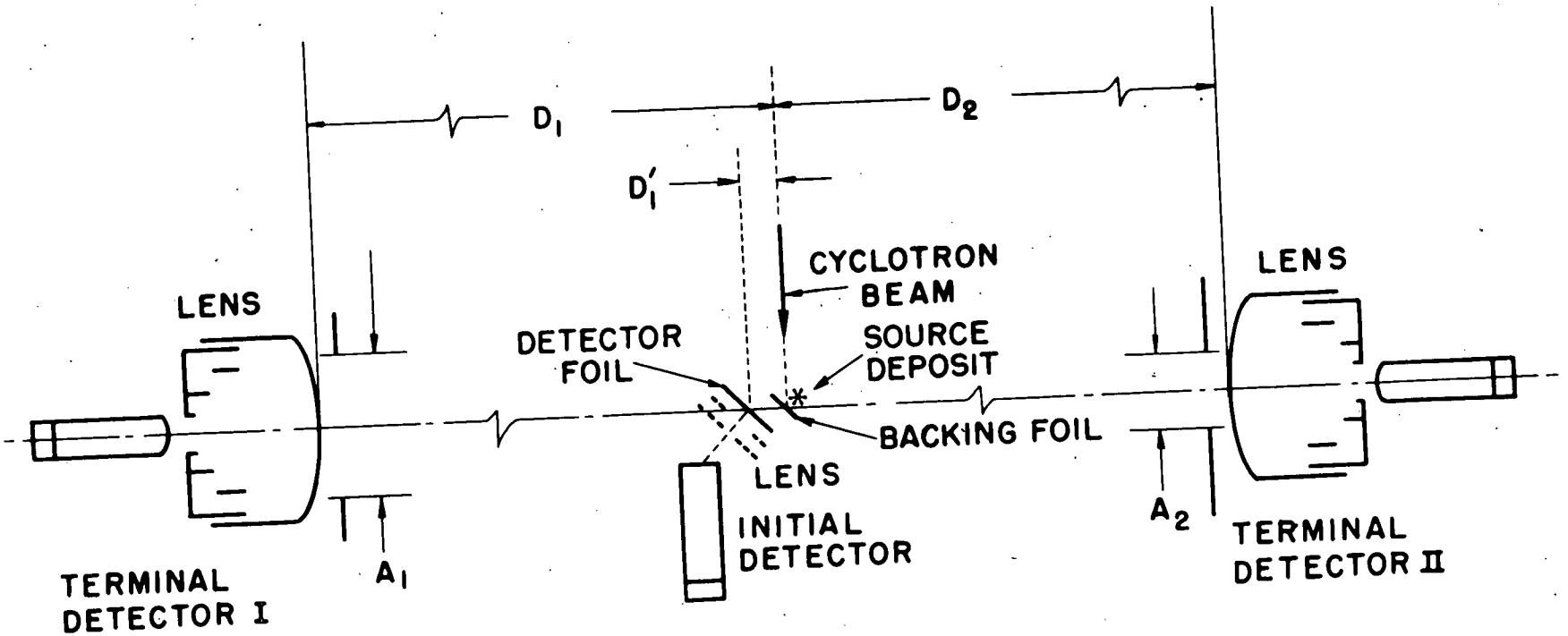

Fig. 2

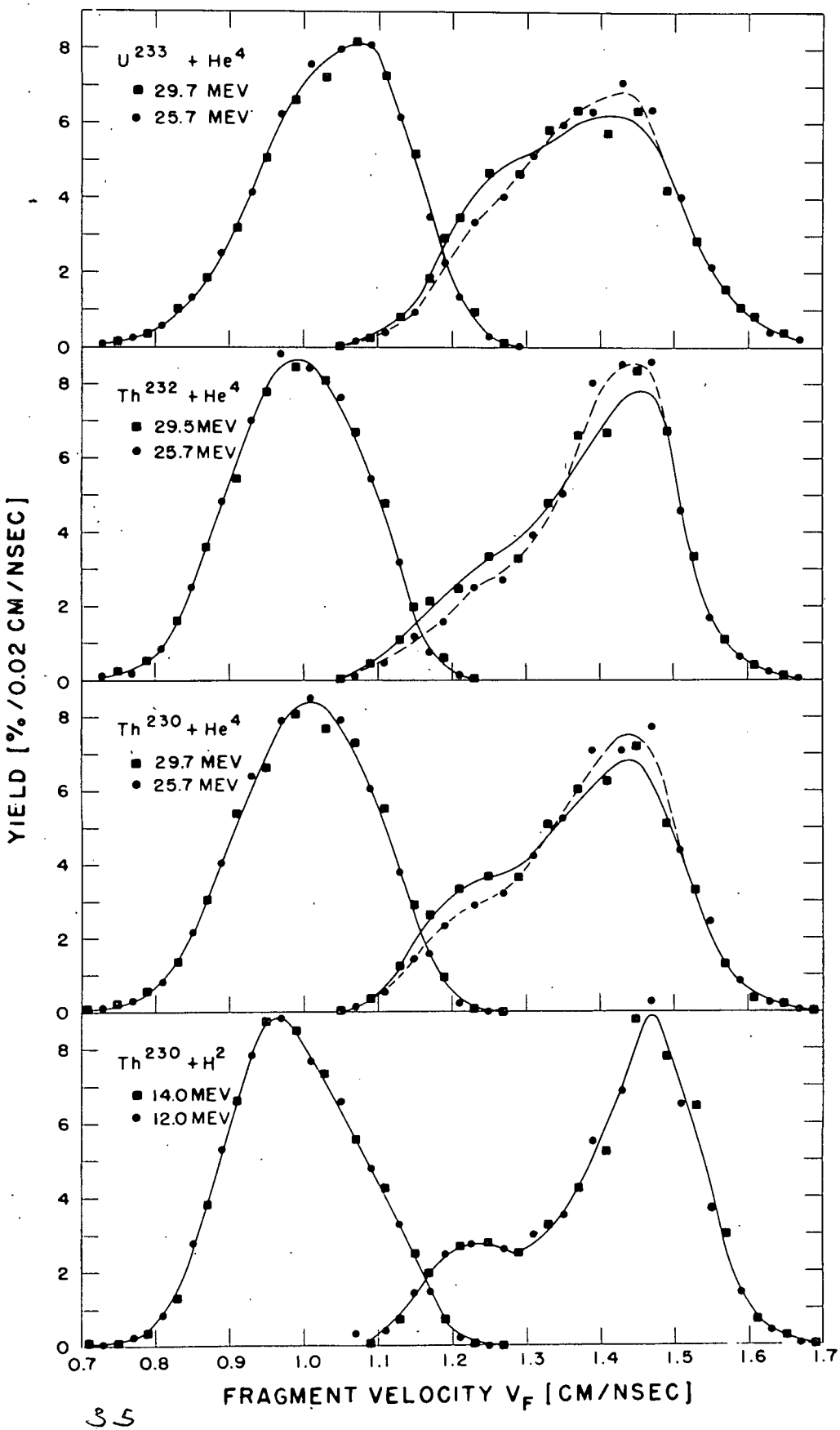
U 233 + He 4
29.7 MEV
25.7 MEV
Th 232 + He 4
29.5MEV
25.7MEV
Th 230 + He 4
29.7 MEV
25.7 MEV
Th 230 + H 2
14.0MEV
12.0MEV
YIELD [%/0.02 CM/NSEC]
FRAGMENT VELOCITY V_F [CM/NSEC]
0.7
0.8
0.9
1.0
1.1
1.2
1.3
1.4
1.5
1.6
1.7

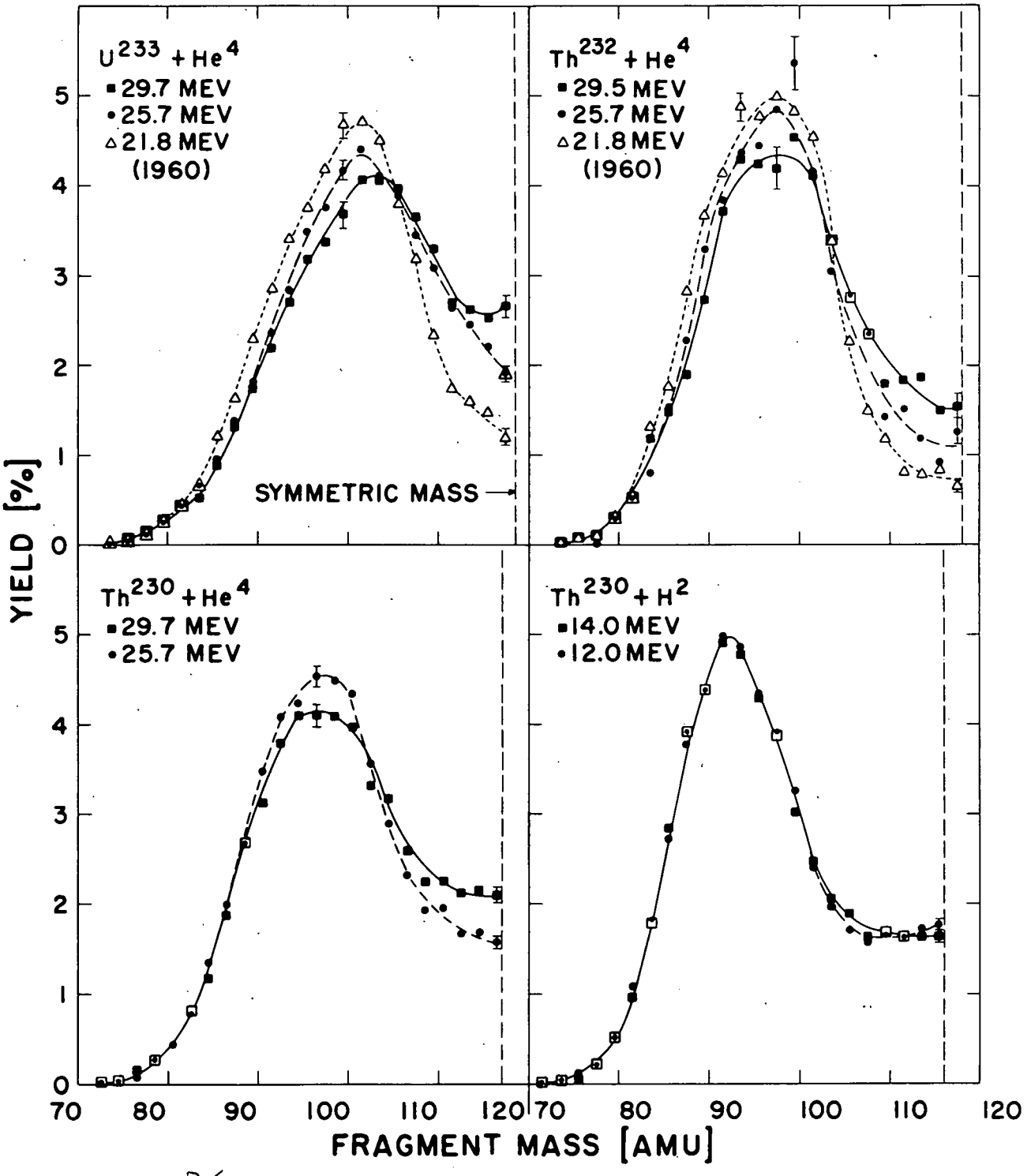
U233 + He4
29.7 MEV
25.7 MEV
21.8 MEV
(1960)
SYMMETRIC MASS
Th232 + He4
29.5 MEV
25.7 MEV
21.8 MEV
(1960)
Th230 + He4
29.7 MEV
25.7 MEV
Th230 + H2
14.0 MEV
12.0 MEV
YIELD [%]
FRAGMENT MASS [AMU]
0
1
2
3
4
5
70
80
90
100
110
120

WHEETSTONE FIG. 4

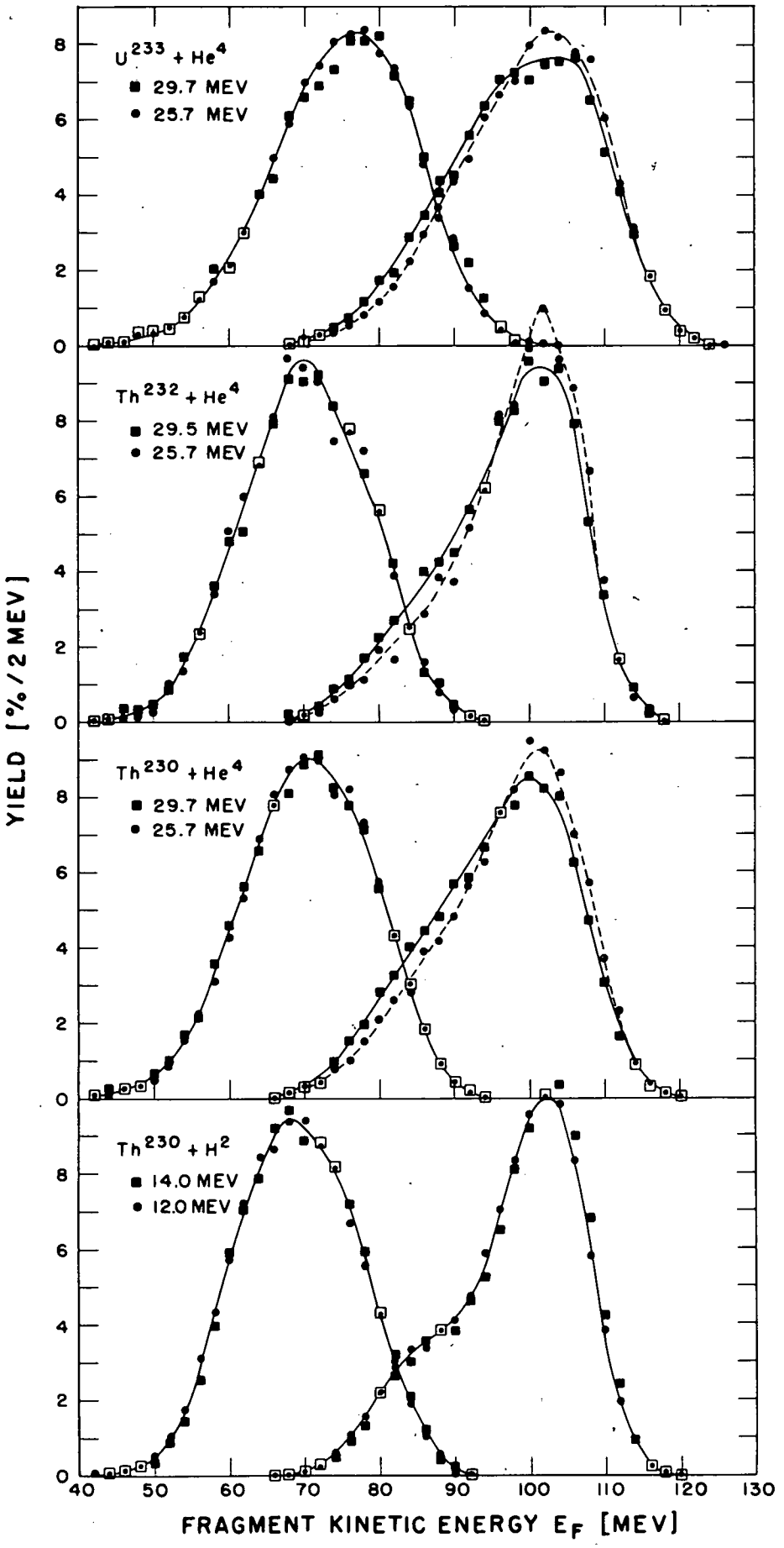

Fig. 5

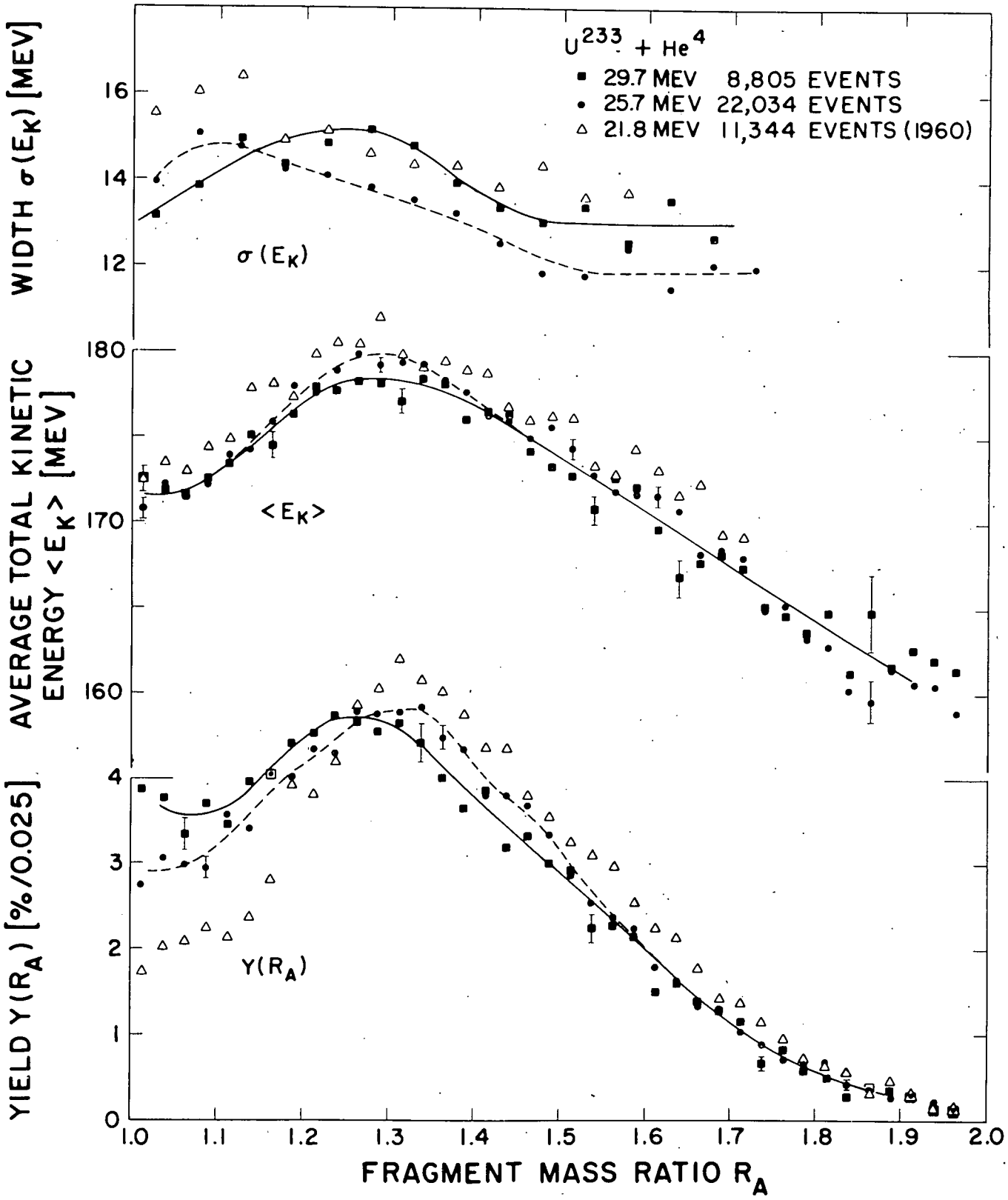
$U^{233} + He^4$
29.7 MEV 8,805 EVENTS
25.7 MEV 22,034 EVENTS
21.8 MEV 11,344 EVENTS (1960)
WIDTH $\sigma(E_K)$ [MEV]
$\sigma(E_K)$
AVERAGE TOTAL KINETIC ENERGY $\langle E_K \rangle$ [MEV]
$\langle E_K \rangle$
YIELD $Y(R_A)$ [%/0.025]
$Y(R_A)$
FRAGMENT MASS RATIO R_A

WHEELER FIG. 6

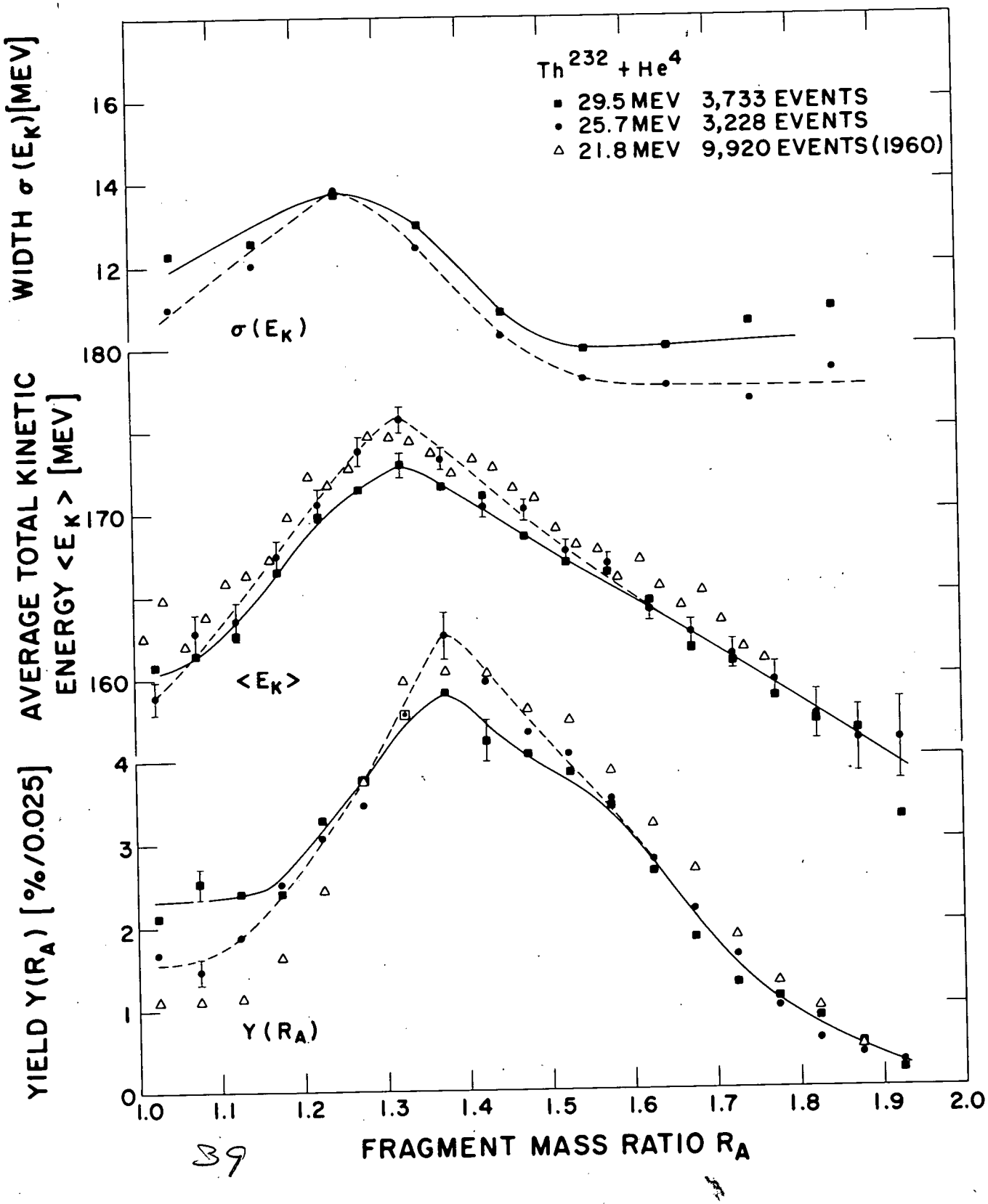

Fig. 7

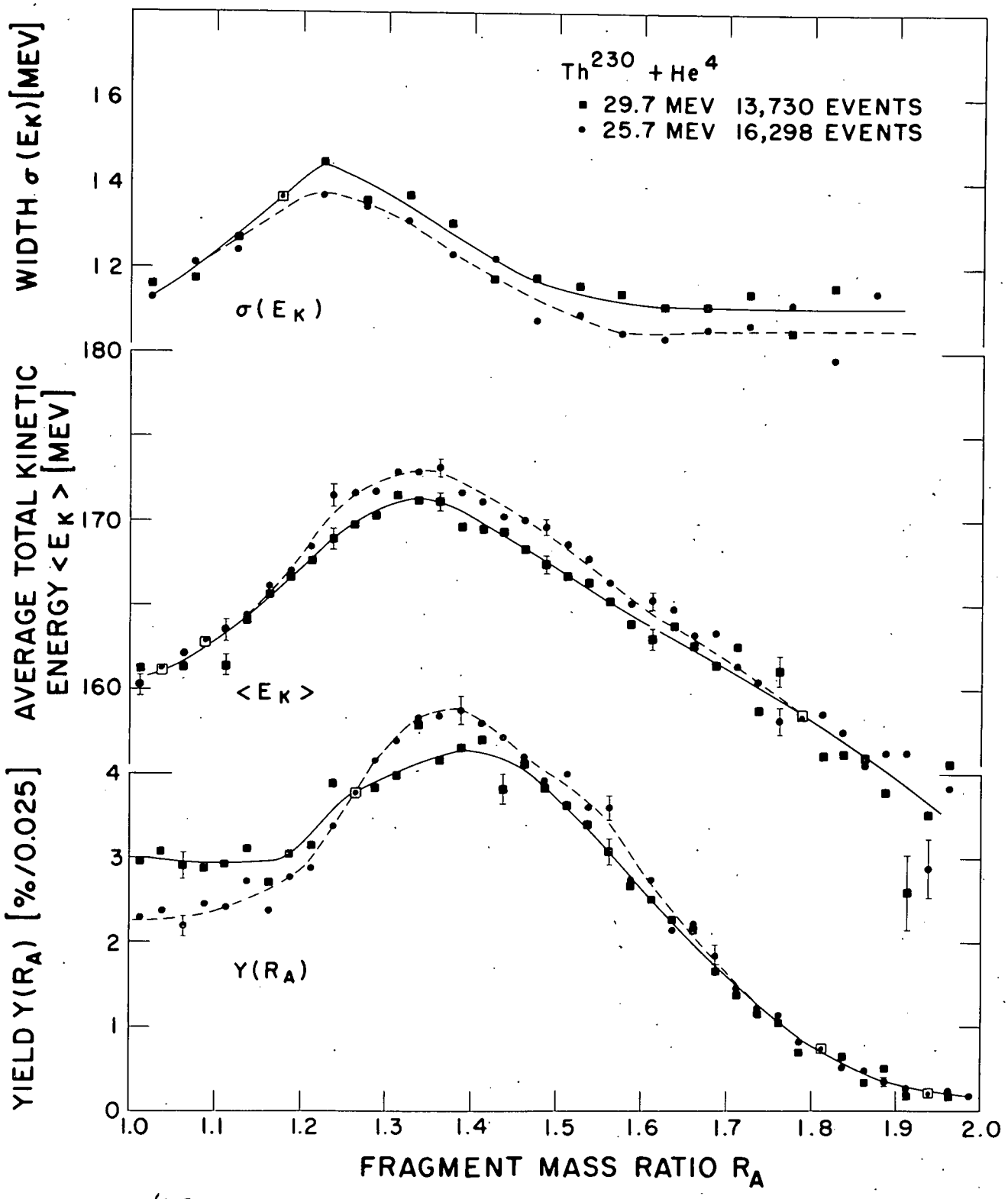
Th230 + He4
29.7 MEV 13,730 EVENTS
25.7 MEV 16,298 EVENTS
WIDTH σ(EK)[MEV]
σ(EK)
AVERAGE TOTAL KINETIC ENERGY <EK> [MEV]
<EK>
YIELD Y(RA) [%/0.025]
Y(RA)
FRAGMENT MASS RATIO RA

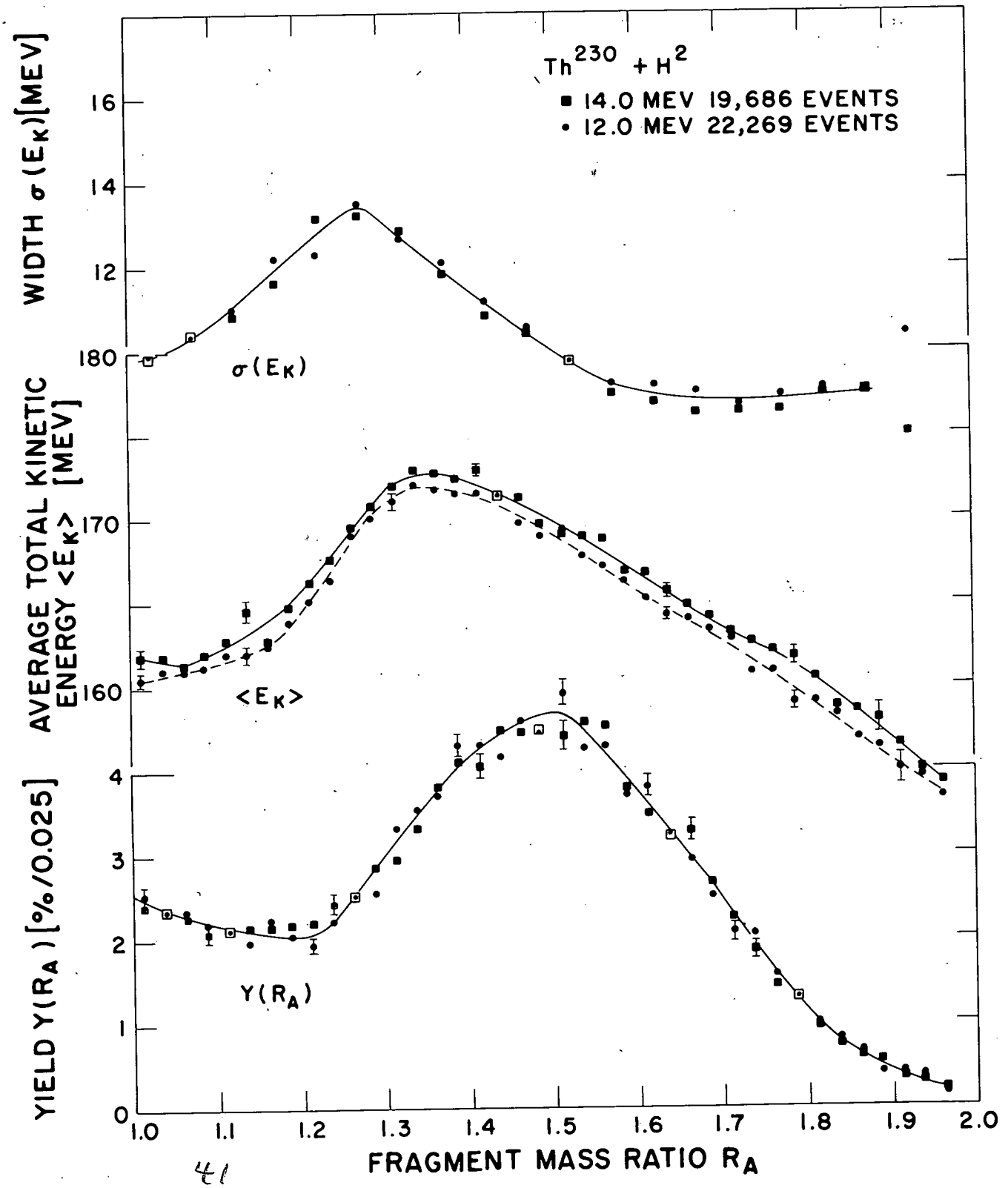
Th230 + H2
■ 14.0 MEV 19,686 EVENTS
• 12.0 MEV 22,269 EVENTS
WIDTH σ(EK)[MEV]
σ(EK)
AVERAGE TOTAL KINETIC ENERGY <EK> [MEV]
<EK>
YIELD Y(RA) [%/0.025]
Y(RA)
FRAGMENT MASS RATIO RA
16
14
12
180
170
160
4
3
2
1
0
1.0
1.1
1.2
1.3
1.4
1.5
1.6
1.7
1.8
1.9
2.0

Fig. 9A

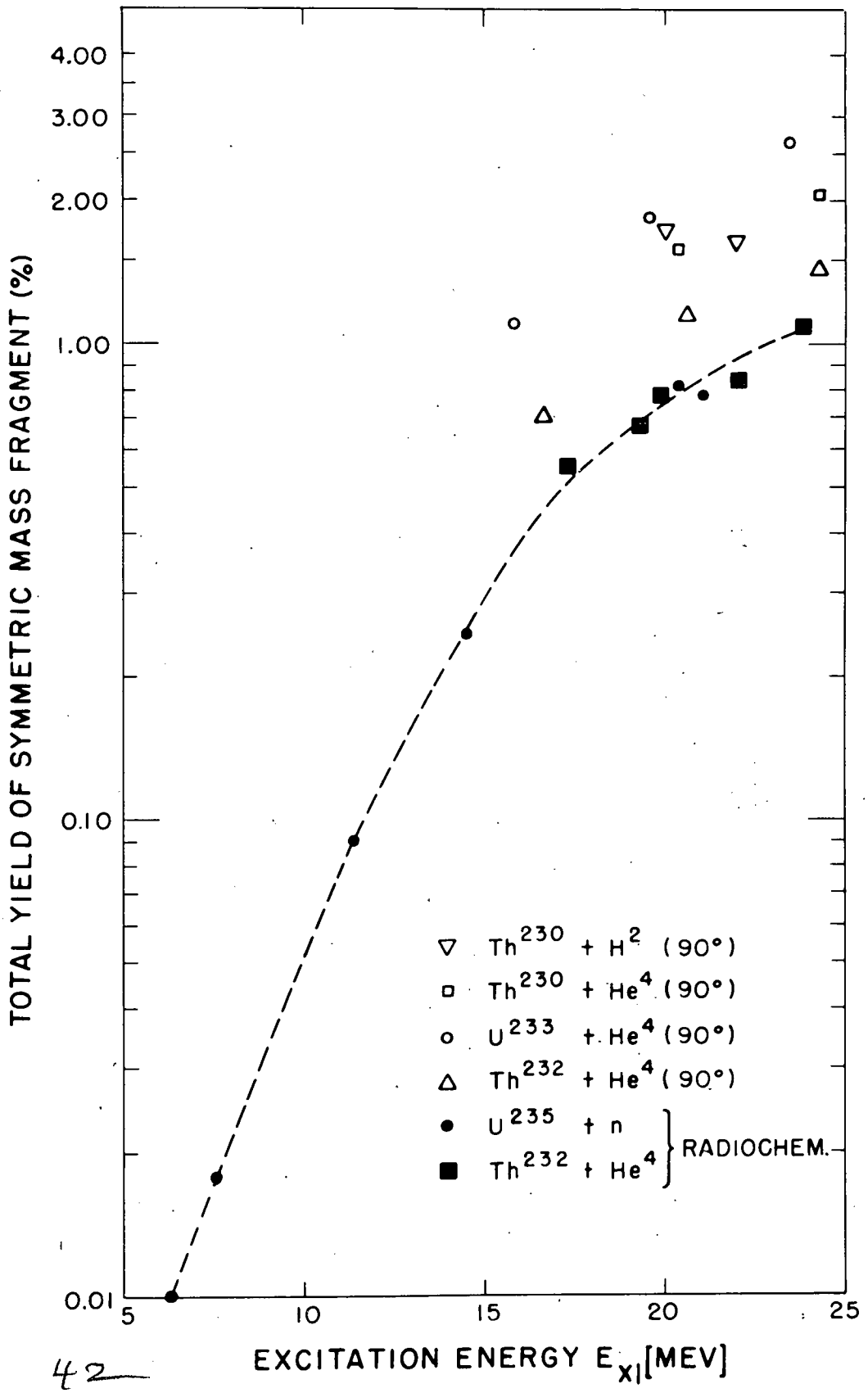
4.00
3.00
2.00
1.00
0.10
0.01
5
10
15
20
25
TOTAL YIELD OF SYMMETRIC MASS FRAGMENT (%)
EXCITATION ENERGY E_{x1} [MEV]
$Th^{230} + H^2$ (90°)
$Th^{230} + He^4$ (90°)
$U^{233} + He^4$ (90°)
$Th^{232} + He^4$ (90°)
$U^{235} + n$
$Th^{232} + He^4$
RADIOCHEM.

WHETSTONE FIG. 9 B.

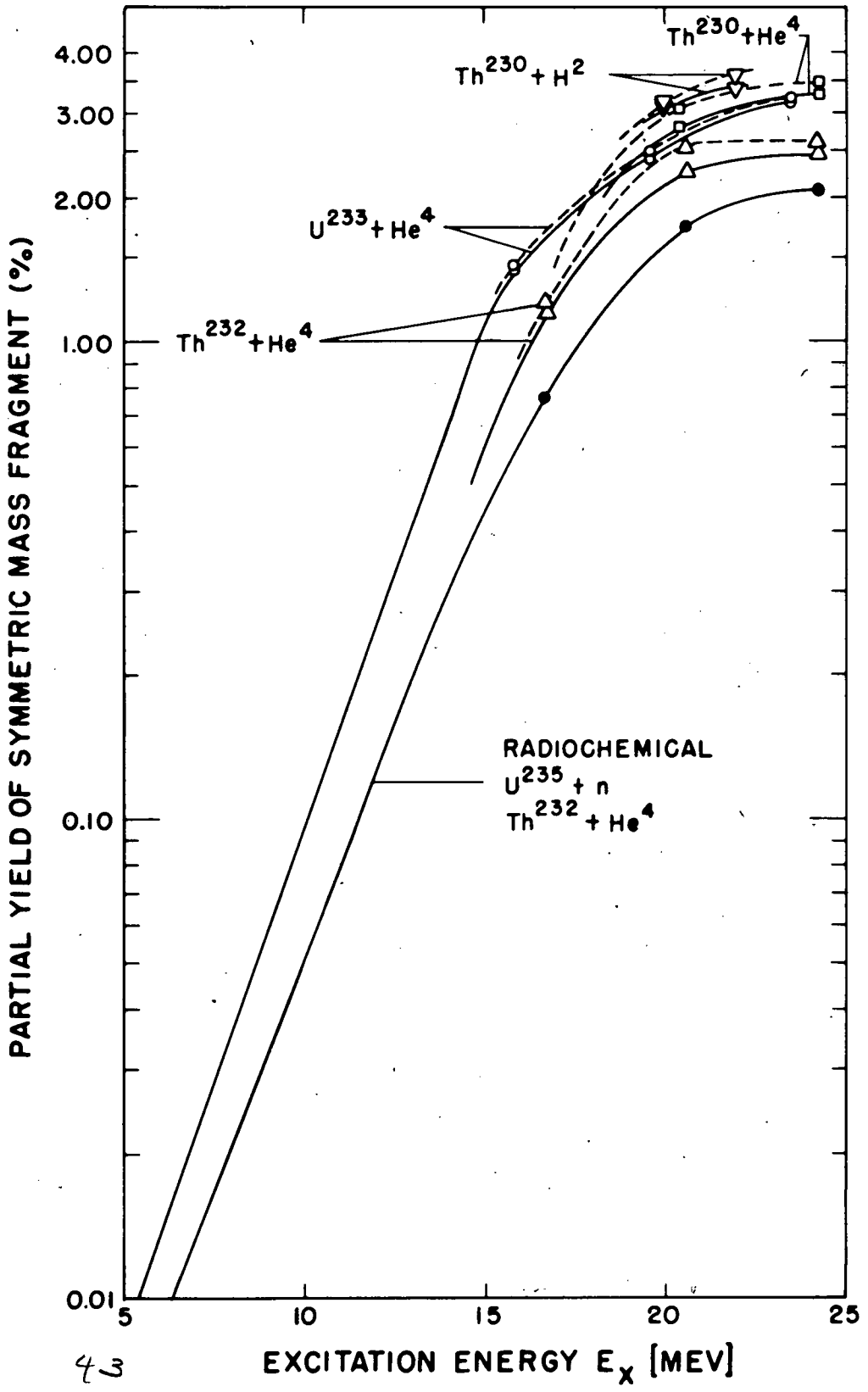

Fig. 10

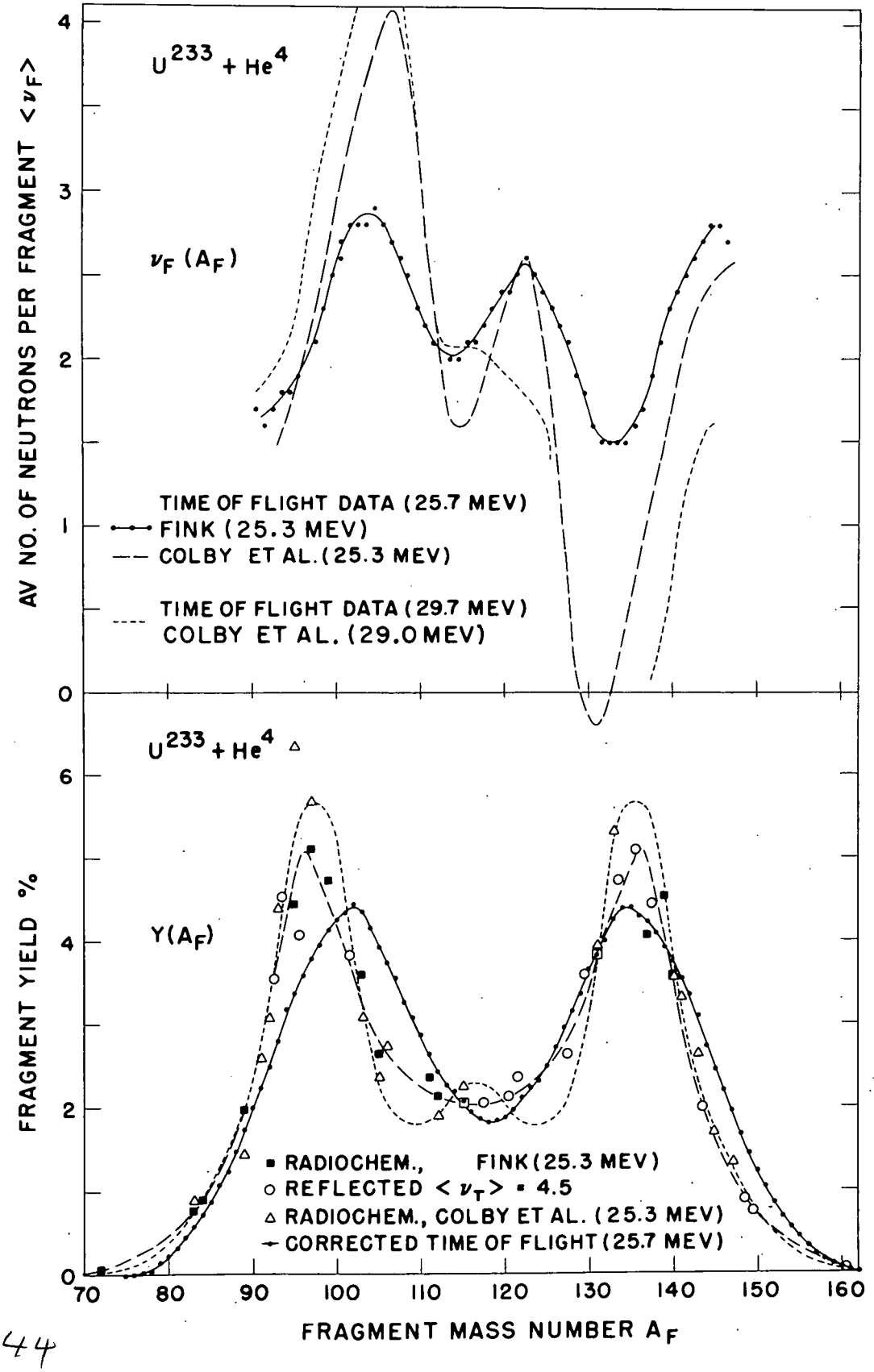
$U^{233} + He^4$
$\nu_F (A_F)$
AV NO. OF NEUTRONS PER FRAGMENT $\langle \nu_F \rangle$
TIME OF FLIGHT DATA (25.7 MEV)
FINK (25.3 MEV)
COLBY ET AL. (25.3 MEV)
TIME OF FLIGHT DATA (29.7 MEV)
COLBY ET AL. (29.0 MEV)
$U^{233} + He^4$ △
$Y(A_F)$
FRAGMENT YIELD %
■ RADIOCHEM., FINK (25.3 MEV)
○ REFLECTED $\langle \nu_T \rangle$ = 4.5
△ RADIOCHEM., COLBY ET AL. (25.3 MEV)
CORRECTED TIME OF FLIGHT (25.7 MEV)
FRAGMENT MASS NUMBER A_F

Fig. 11

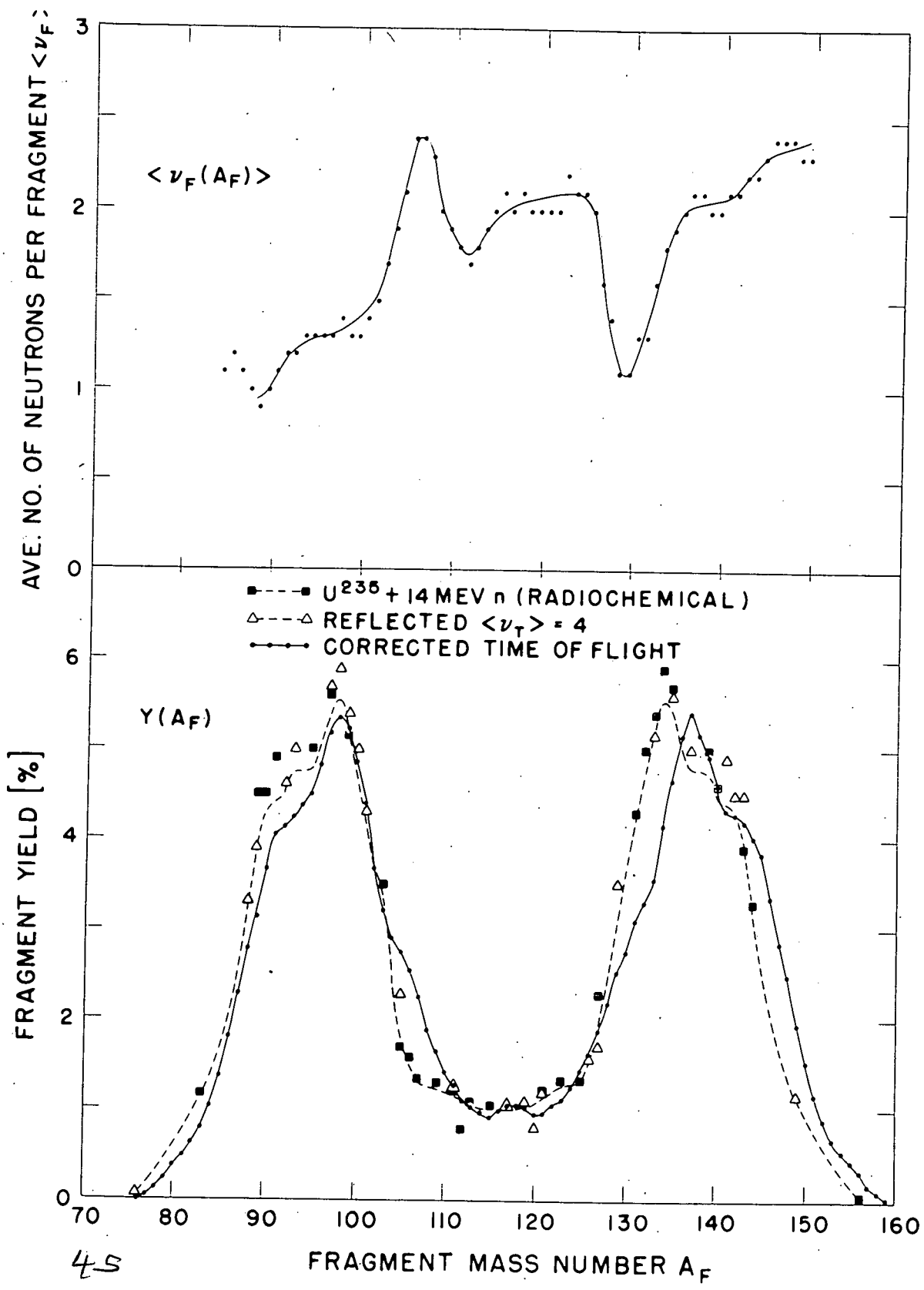
AVE. NO. OF NEUTRONS PER FRAGMENT $\langle \nu_F \rangle$
$\langle \nu_F(A_F) \rangle$
U^{235} + 14 MEV n (RADIOCHEMICAL)
REFLECTED $\langle \nu_T \rangle = 4$
CORRECTED TIME OF FLIGHT
$Y(A_F)$
FRAGMENT YIELD [%]
FRAGMENT MASS NUMBER A_F
0
1
2
3
4
6
70
80
90
100
110
120
130
140
150
160